




Unified Interpretation of 95 GeV Excesses in the Two Higgs Doublet type II Seesaw Model

Brahim Ait-Ouazghour ^{1*}, Mohamed Chabab ^{1,2†}, Khalid Goure ^{1‡}

¹LPHEA, Faculty of Science Semlalia, Cadi Ayyad University, P.O.B. 2390
Marrakech, Morocco.

² National School of Applied Science, P.O.B 63 Saffi 46000, Morocco

Abstract

In the search for a light Higgs boson, the ATLAS and CMS experiments have observed excesses in both the diphoton ($\gamma\gamma$) and di-tau-pair ($\tau^+\tau^-$) decay channels at about 95 GeV. The LEP collaboration has also previously reported an excess in the $b\bar{b}$ channel at a comparable Higgs mass. In this paper, we explore whether these excesses can be accommodated within the framework of the Two Higgs Doublet type II Seesaw Model (2HDMcT). By implementing various theoretical constraints and experimental limits on the parameter space, we first demonstrate that a light CP-even Higgs boson, h_1 , with a mass around 95 GeV can simultaneously account for the excesses observed in the $\gamma\gamma$ and $b\bar{b}$ channels, provided a Type I Yukawa texture is employed. More interestingly, our analysis shows that the three excesses in $\gamma\gamma$, $b\bar{b}$ and $\tau^+\tau^-$ channels can well be accommodated simultaneously, reaching a 0.64σ C.L. if the CP-odd Higgs boson A_1 is nearly mass degenerate and superposed to the light CP-even Higgs h_1 .

1 Introduction

The discovery of the 125 GeV Higgs boson by the ATLAS and CMS collaborations [1–3] marks an important milestone in the quest to unravel the nature of electroweak symmetry breaking (EWSB). This discovery established the Standard Model (SM) as a robust and successful framework for describing the fundamental particles and their interactions. Though the SM predictions have been rigorously tested [4, 5], it still faces challenges since it failed to account for several physical phenomena, such as: the origin of dark matter [6, 7], the hierarchy problem [8], and the neutrino mass generation [9, 10]. To tackle these deficiencies, numerous theoretical frameworks, beyond the Standard Model (BSM) have been suggested in the literature. BSM scenarios with an extended Higgs sector are among the most popular ones. The fermion sector of the SM being non minimal, it is legitimate to suggest scenarios with an extended scalar sector, hence a rich Higgs spectrum, aiming to accommodate new physics. Further investigation of EWSB, precise determination of the properties of the observed 125 GeV Higgs and the searches for new scalar particles are actively conducted at the LHC. Among important key focus of the recent experimental physics programs

*b.ouazghour@gmail.com

†mchabab@uca.ac.ma (Corresponding author)

‡khalidgoure01@gmail.com

are the observation of additional Higgs bosons with light mass below 125 GeV LEP [11–13], Tevatron [14] and LHC [15–23]. These searches have been performed on different Higgs decay channels: based on the 8 TeV data and Run 2 first year data at 13 TeV, corresponding to an integrated luminosity of 19.7 fb^{-1} and 35.9 fb^{-1} , respectively, CMS results first revealed a local excess of 2.8σ at 95.3 GeV [16]. Later, the CMS collaboration using the full Run 2 data set, reported a local excess of 2.9σ at 95.4 GeV [20, 22]. Similarly the ATLAS experiment searching for diphoton resonances using 140 fb^{-1} of pp collisions, found a local excess of 1.7σ around 95 GeV [23, 24]. Besides the di-photon excess, another excess in the $\tau^-\tau^+$ channel has been observed by CMS [25]. Notably, many years ago, LEP also reported a comparable local 2.3σ excess in the $e^+e^- \rightarrow Z(\phi \rightarrow b\bar{b})$ channel [12]. So, these observations deserve further phenomenological investigations within BSM models, in particular, to see whether the excesses can be interpreted via scalar particles at about 95 GeV in their extended Higgs sectors. Many attempts have been performed in different theoretical frameworks [26–69].

In this work, our analysis is done within the framework of the Two Higgs Doublet Type II seesaw Model (2HDMcT). Besides the two Higgs doublets with hypercharge $Y = 1$, The Two Higgs Doublet Model (2HDM) is augmented with an $SU(2)_L$ complex scalar triplet Δ with $Y_\Delta = 2$. Due to the similarity between mass generation from the seesaw mechanism and the Brout-Englert-Higgs mechanism, the 2HDMcT model is highly attractive: it exhibits numerous phenomenological features, particularly distinct from those arising in the scalar sector of the 2HDM. Apart its broader spectrum in comparison to 2HDM, it is arguably among the simplest and well motivated frameworks that can explain either all neutrino oscillation data in a gauge-invariant way [70–73], or the dark matter origin [74]. In addition to that, the doubly charged Higgs H^{++} is considered a smoking gun of 2HDMcT, H^{++} being intensively searched for at ATLAS and CMS through promising $H^{++}H^{--}$ and $H_i^+H_i^-$ ($i = 1, 2$) channels decaying to the same sign di-lepton [75]. Moreover beyond the Higgs phenomenology, it has been demonstrated that interactions between doublet and triplet fields in this model can induce a strong first order electroweak phase transition, hence providing conditions for the generation of the baryon asymmetry through electroweak baryogenesis [76]. Furthermore, this model provides other appealing features including possibility of enhanced Higgs couplings, modified Higgs decay channels, and the presence of additional scalar particles that can be probed at current or future colliders. As an example, besides contributions from SM charged particles (W^\pm , and fermions), the loop-mediated decay $h_1 \rightarrow \gamma\gamma$ receives extra contributions from the singly and doubly charged Higgs bosons, predicted by 2HDMcT spectrum [77]. This could increase the branching ratio $\mathcal{BR}_{2\text{HDMcT}}(h_1 \rightarrow \gamma\gamma)$ (For more details see Appendix 4). Thus the aim of this paper is to investigate whether the 2HDMcT, with its broader spectrum compared to simpler models, can account for the reported excesses [12, 22, 23].

To perform a rigorous study, we have implemented a full set of theoretical constraints originated from perturbative unitarity, and electroweak vacuum stability. To accommodate the 125 GeV Higgs boson h_{125} we implement the HiggsTools package [78] subpackage HiggsSignals [78–81]. Also to guarantee that the allowed parameter space aligns with exclusion limits resulting from searches for additional Higgs bosons at the LHC and LEP, the subpackage HiggsBounds [78, 82–85] is employed. In addition, the 2HDMcT parameter space is further constrained by electroweak precision observables and the $\bar{B} \rightarrow X_s\gamma$ constraint at 95% C.L.

The paper is organized as follows. In Sec.2, we briefly introduce the 2HDMcT, specifically focusing on the CP-even scalar spectrum. In Sec.3, we first provide a brief discussion of the relevant theoretical and experimental constraints delimiting our model parameter space, then we

present our analysis and results. Sect.4 is devoted to our conclusion.

2 The model: 2HDMcT

2HDMcT includes two Higgs doublets with a hypercharge $Y = +1$ and one complex scalar triplet with $Y = +2$. After the electroweak symmetry is spontaneously broken, these fields can be parameterized as :

$$\Phi_1 = \begin{pmatrix} \phi_1^+ \\ \phi_1^0 \end{pmatrix}, \quad \Phi_2 = \begin{pmatrix} \phi_2^+ \\ \phi_2^0 \end{pmatrix}, \quad \Delta = \begin{pmatrix} \delta^+/\sqrt{2} & \delta^{++} \\ (v_t + \delta^0 + i\eta_0)/\sqrt{2} & -\delta^+/\sqrt{2} \end{pmatrix} \quad (1)$$

with $\phi_1^0 = (v_1 + \psi_1 + i\eta_1)/\sqrt{2}$, $\phi_2^0 = (v_2 + \psi_2 + i\eta_2)/\sqrt{2}$ and $\sqrt{v_1^2 + v_2^2 + 2v_t^2} = 246$ GeV, where v_1, v_2 and v_t are the vacuum expectation values of the two Higgs doublet and triplet fields respectively.

The most general $SU(2)_L \times U(1)_Y$ invariant Lagrangian of 2HDMcT is given by:

$$\mathcal{L} = \sum_{i=1}^2 (D_\mu \Phi_i)^\dagger (D^\mu \Phi_i) + \text{Tr}(D_\mu \Delta)^\dagger (D^\mu \Delta) - V(\Phi_i, \Delta) + \mathcal{L}_{\text{Yukawa}} \quad (2)$$

where the covariant derivatives are defined as,

$$D_\mu \Phi_i = \partial_\mu \Phi_i + ig T^a W_\mu^a \Phi_i + i \frac{g'}{2} B_\mu \Phi_i \quad (3)$$

$$D_\mu \Delta = \partial_\mu \Delta + ig [T^a W_\mu^a, \Delta] + i g' \frac{Y_\Delta}{2} B_\mu \Delta \quad (4)$$

(W_μ^a , g), and (B_μ , g') denoting respectively the $SU(2)_L$ and $U(1)_Y$ gauge fields and couplings and $T^a \equiv \sigma^a/2$, with σ^a ($a = 1, 2, 3$) the Pauli matrices. In terms of the two $SU(2)_L$ Higgs doublets Φ_i and the triplet field Δ , the 2HDMcT scalar potential is given by [75, 86]:

$$\begin{aligned} V(\Phi_1, \Phi_2, \Delta) = & m_{11}^2 \Phi_1^\dagger \Phi_1 + m_{22}^2 \Phi_2^\dagger \Phi_2 - [m_{12}^2 \Phi_1^\dagger \Phi_2 + \text{h.c.}] + \frac{\lambda_1}{2} (\Phi_1^\dagger \Phi_1)^2 + \frac{\lambda_2}{2} (\Phi_2^\dagger \Phi_2)^2 \\ & + \lambda_4 (\Phi_1^\dagger \Phi_2)(\Phi_2^\dagger \Phi_1) + \left\{ \frac{\lambda_5}{2} (\Phi_1^\dagger \Phi_2)^2 + [\beta_1 (\Phi_1^\dagger \Phi_1) + \beta_2 (\Phi_2^\dagger \Phi_2)] \Phi_1^\dagger \Phi_2 + \text{h.c.} \right\} \\ & + \lambda_3 (\Phi_1^\dagger \Phi_1)(\Phi_2^\dagger \Phi_2) + \lambda_6 \Phi_1^\dagger \Phi_1 \text{Tr} \Delta^\dagger \Delta + \lambda_7 \Phi_2^\dagger \Phi_2 \text{Tr} \Delta^\dagger \Delta \\ & + \left\{ \mu_1 \Phi_1^T i \sigma^2 \Delta^\dagger \Phi_1 + \mu_2 \Phi_2^T i \sigma^2 \Delta^\dagger \Phi_2 + \mu_3 \Phi_1^T i \sigma^2 \Delta^\dagger \Phi_2 + \text{h.c.} \right\} + \lambda_8 \Phi_1^\dagger \Delta \Delta^\dagger \Phi_1 \\ & + \lambda_9 \Phi_2^\dagger \Delta \Delta^\dagger \Phi_2 + m_\Delta^2 \text{Tr}(\Delta^\dagger \Delta) + \bar{\lambda}_8 (\text{Tr} \Delta^\dagger \Delta)^2 + \bar{\lambda}_9 \text{Tr}(\Delta^\dagger \Delta)^2 \end{aligned}$$

In this work, we avoid tree-level Higgs mediated $FCNC_s$ by considering Z_2 symmetry ($\Phi_1 \rightarrow +\Phi_1$ and $\Phi_2 \rightarrow -\Phi_2$) with $\beta_1 = \beta_2 = 0$. The Z_2 symmetry is softly broken by the bi-linear terms proportional to m_{12}^2 , μ_1 , μ_2 and μ_3 parameters. In addition, we assume that m_{11}^2 , m_{22}^2 , m_Δ^2 , m_{12}^2 , λ_i ($i = 1, \dots, 9$), $\bar{\lambda}_j$ ($j = 8, 9$), μ_k ($k = 1, \dots, 3$), $\beta_{1,2}$ are real potential parameters. In the CP-even

scalar sector, the mixing of the states (ρ_1, ρ_2, ρ_0) leads to a total of three CP-even physical Higgs bosons (h_1, h_2, h_3) . The neutral scalar mass matrix reads as,

$$\mathcal{M}_{\mathcal{CP}_{even}}^2 = \begin{pmatrix} m_{\rho_1\rho_1}^2 & m_{\rho_2\rho_1}^2 & m_{\rho_0\rho_1}^2 \\ m_{\rho_1\rho_2}^2 & m_{\rho_2\rho_2}^2 & m_{\rho_0\rho_2}^2 \\ m_{\rho_1\rho_0}^2 & m_{\rho_2\rho_0}^2 & m_{\rho_0\rho_0}^2 \end{pmatrix} \quad (5)$$

where the diagonal terms are given by,

$$\begin{aligned} m_{\rho_1\rho_1}^2 &= \lambda_1 v_1^2 + \frac{v_2 (\sqrt{2}m_3^2 + \mu_3 v_t)}{\sqrt{2}v_1} \\ m_{\rho_2\rho_2}^2 &= \lambda_2 v_2^2 + \frac{v_1 (\sqrt{2}m_3^2 + \mu_3 v_t)}{\sqrt{2}v_2} \\ m_{\rho_0\rho_0}^2 &= \frac{4(\bar{\lambda}_8 + \bar{\lambda}_9) v_t^3 + \sqrt{2}(\mu_1 v_1^2 + \mu_3 v_2 v_1 + \mu_2 v_2^2)}{2v_t} \end{aligned} \quad (6)$$

while the off-diagonal terms are,

$$\begin{aligned} m_{\rho_2\rho_1}^2 &= m_{\rho_1\rho_2}^2 = \frac{1}{\sqrt{2}} \left(\sqrt{2}v_1 v_2 \lambda_{345} - \sqrt{2}m_3^2 - \mu_3 v_t \right) \\ m_{\rho_0\rho_1}^2 &= m_{\rho_1\rho_0}^2 = \frac{1}{\sqrt{2}} \left(\sqrt{2}v_1 v_t (\lambda_6 + \lambda_8) - (2\mu_1 v_1 + \mu_3 v_2) \right) \\ m_{\rho_0\rho_2}^2 &= m_{\rho_2\rho_0}^2 = \frac{1}{\sqrt{2}} \left(\sqrt{2}v_2 v_t (\lambda_7 + \lambda_9) - (2\mu_2 v_2 + \mu_3 v_1) \right) \end{aligned} \quad (7)$$

$\mathcal{M}_{\mathcal{CP}_{even}}^2$ mass matrix can be diagonalized by an orthogonal matrix \mathcal{E} parametrized as,

$$\mathcal{E} = \begin{pmatrix} c_{\alpha_1} c_{\alpha_2} & s_{\alpha_1} c_{\alpha_2} & s_{\alpha_2} \\ -(c_{\alpha_1} s_{\alpha_2} s_{\alpha_3} + s_{\alpha_1} c_{\alpha_3}) & c_{\alpha_1} c_{\alpha_3} - s_{\alpha_1} s_{\alpha_2} s_{\alpha_3} & c_{\alpha_2} s_{\alpha_3} \\ -c_{\alpha_1} s_{\alpha_2} c_{\alpha_3} + s_{\alpha_1} s_{\alpha_3} & -(c_{\alpha_1} s_{\alpha_3} + s_{\alpha_1} s_{\alpha_2} c_{\alpha_3}) & c_{\alpha_2} c_{\alpha_3} \end{pmatrix} \quad (8)$$

where the mixing angles α_1, α_2 and α_3 vary within the ranges :

$$-\frac{\pi}{2} \leq \alpha_{1,2,3} \leq \frac{\pi}{2}. \quad (9)$$

The rotation between the two basis (ρ_1, ρ_2, ρ_0) and (h_1, h_2, h_3) diagonalizes the mass matrix $\mathcal{M}_{\mathcal{CP}_{even}}^2$ as,

$$\mathcal{E} \mathcal{M}_{\mathcal{CP}_{even}}^2 \mathcal{E}^T = \text{diag}(m_{h_1}^2, m_{h_2}^2, m_{h_3}^2) \quad (10)$$

yielding three mass eigenstates, ordered as :

$$m_{h_1}^2 < m_{h_2}^2 < m_{h_3}^2 \quad (11)$$

The Yukawa Lagrangian $\mathcal{L}_{\text{Yukawa}}$ encompasses the entire Yukawa sector of the $2HDM$ along with an additional Yukawa term originating from the triplet field. The latter generates mass terms for the neutrinos, after spontaneous symmetry breaking.

$$-\mathcal{L}_{\text{Yukawa}} \supset -Y_\nu L^T C \otimes i\sigma^2 \Delta L + \text{h.c.} \quad (12)$$

	$C_U^{h_1}$	$C_D^{h_1}$	$C_l^{h_1}$	$C_U^{h_2}$	$C_D^{h_2}$	$C_l^{h_2}$	$C_U^{h_3}$	$C_D^{h_3}$	$C_l^{h_3}$
Type-I	$\frac{\mathcal{E}_{12}}{s_\beta}$	$\frac{\mathcal{E}_{12}}{s_\beta}$	$\frac{\mathcal{E}_{12}}{s_\beta}$	$\frac{\mathcal{E}_{22}}{s_\beta}$	$\frac{\mathcal{E}_{22}}{s_\beta}$	$\frac{\mathcal{E}_{22}}{s_\beta}$	$\frac{\mathcal{E}_{32}}{s_\beta}$	$\frac{\mathcal{E}_{32}}{s_\beta}$	$\frac{\mathcal{E}_{32}}{s_\beta}$

Table 1: Normalized Yukawa couplings coefficients of the CP-even h_i neutral Higgs bosons to the leptons, up and down quarks (u, d) in 2HDMcT.

	$C_W^{h_i}$	$C_Z^{h_i}$
h_1	$\frac{v_1}{v}\mathcal{E}_{11} + \frac{v_2}{v}\mathcal{E}_{21} + 2\frac{v_t}{v}\mathcal{E}_{31}$	$\frac{v_1}{v}\mathcal{E}_{11} + \frac{v_2}{v}\mathcal{E}_{21} + 4\frac{v_t}{v}\mathcal{E}_{31}$

Table 2: The normalized couplings of the neutral \mathcal{CP}_{even} h_1 Higgs boson to the massive gauge bosons $V = W, Z$ in 2HDMcT.

where L and Y_ν denote $SU(2)_L$ doublets of left-handed leptons and neutrino Yukawa couplings, respectively. C is the charge conjugation operator. Furthermore, in terms of the various α_i which appear in the expressions of \mathcal{E}_{ij} matrix elements, we list in Table 1, the three \mathcal{CP}_{even} Higgs bosons Yukawa couplings for different Yukawa textures.

On the other hand, by expanding the covariant derivative D_μ and by performing the usual transformations of the gauge and scalar fields, one can identify the Higgs couplings h_i to the massive gauge bosons $V = W, Z$ as given in Table 2, where the two couplings $C_W^{h_i}$ and $C_Z^{h_i}$ differ only by a factor 2 associated to v_t . Note that in 2HDMcT new contributions show up due to the triplet field Δ coupling to the SM particles,

3 Constraints and Numerical Results

In this section we first present a summary of the theoretical and experimental constraints imposed on the model parameter space [75, 87], then we proceed with an overview of our analysis and discuss the relevant details of the results, aiming to determine whether the various excesses observed at about near 95 GeV can be interpreted as the decay signal of the lighter neutral scalar h_1 predicted in 2HDMcT. Here, the h_2 state is chosen to mimic the 125 GeV observed Higgs boson [1, 2]. Subsequently our analysis will be performed using the type-I Yukawa texture,[§] and the full set of the following theoretical constraints [75, 87] and Higgs exclusion limits:

- **Unitarity** : The scattering processes must obey the perturbative unitarity.
- **Perturbativity**: The quartic couplings of the scalar potential are constrained by the following conditions: $|\lambda_i| < 8\pi$ for each $i = 1, \dots, 5$.

[§]The other Yukawa textures are unable to explain these excesses: In the parameter space of 2HDMcT Types II, III, and IV, the points that satisfy all constraints fall well outside the 2σ ellipse, and thus cannot account for the observed excesses.

Observable	Experimental result	95% C.L.
$\text{BR}(\bar{B} \rightarrow X_s \gamma)$ [87]	$(3.49 \pm 0.19) \times 10^{-4}$ [91]	$[3.11 \times 10^{-4}, 3.87 \times 10^{-4}]$

Table 3: Experimental result of flavor observable: $\bar{B} \rightarrow X_s \gamma$ at 95% C.L.

- **Vacuum stability** : Boundedness from below BFB arising from the positivity in any direction of the fields Φ_i , Δ .
- **Electroweak precision observables**: The oblique parameters S, T and U [88, 89] have been calculated in 2HDMcT [87]. The analysis of the precision electroweak data in light of the new PDG mass of the W boson yields [90]:

$$S^{exp} = -0.01 \pm 0.07, \quad T^{exp} = 0.04 \pm 0.06 \quad \rho_{ST} = +0.92. \quad (13)$$

We use the following χ_{ST}^2 test :

$$\begin{aligned} \chi_{ST}^2 &= \frac{1}{\hat{\sigma}_{T1}^2(1 - \rho_{ST}^2)}(T - T^{exp})^2 + \frac{1}{\hat{\sigma}_{S1}^2(1 - \rho_{ST}^2)}(S - S^{exp})^2 \\ &- \frac{2\rho_{ST}}{\hat{\sigma}_T \hat{\sigma}_S(1 - \rho_{ST}^2)}(T - T^{exp})(S - S^{exp}) \leq R^2, \end{aligned} \quad (14)$$

with $R^2 = 2.3$ and 5.99 corresponding to 68.3% and 95% confidence levels (C.L.) respectively. Our numerical analysis is performed with χ_{ST}^2 at 95% C.L.

- To further delimit the allowed parameter space, the **HiggsTools** package [78] is employed. This ensures that the allowed parameter regions align with the observed properties of the 125 GeV Higgs boson (**HiggsSignals** [78–81]) and with the exclusion limits from additional Higgs bosons search at the LHC and at LEP (**HiggsBounds** [78, 82–85]).
- **Flavour constraints**: Flavour constraints are also implemented in our analysis by using the B -physics results derived in [87] and the experimental data at 2σ [91] shown in Table 3.

Our analysis is performed using the following input parameters in 2HDMcT,

$$\mathcal{P}_I = \{\alpha_1, \alpha_2, \alpha_3, m_{h_1}, m_{h_2}, \lambda_1, \lambda_3, \lambda_4, \lambda_6, \lambda_7, \lambda_8, \lambda_9, \bar{\lambda}_8, \bar{\lambda}_9, \mu_1, v_t, \tan \beta\} \quad (15)$$

in the following ranges,

$$\begin{aligned} 93 \text{ GeV} \leq m_{h_1} \leq 97 \text{ GeV}, \quad m_{h_1} \leq m_{h_2} \leq m_{h_3} \leq 1 \text{ TeV}, \quad 80 \text{ GeV} \leq m_{A_1} \leq m_{A_2} \leq 1 \text{ TeV} \\ 80 \text{ GeV} \leq m_{H^{\pm\mp}} \leq 1 \text{ TeV}, \quad 80 \text{ GeV} \leq m_{H_1^\pm} \leq m_{H_2^\pm} \leq 1 \text{ TeV}, \quad m_{h_2} = 125.09 \text{ GeV}, \quad \frac{-\pi}{2} \leq \alpha_1 \leq \frac{\pi}{2}, \quad -0.1 \leq \alpha_{2,3} \leq 0.1 \\ 0.5 \leq \tan \beta = v_2/v_1 \leq 30, \quad -10^2 \leq \mu_1 \leq 10^2, \quad 0 \leq v_t \leq 1 \text{ GeV} \quad -8\pi \leq \lambda_i, \bar{\lambda}_i \leq 8\pi, \end{aligned} \quad (16)$$

We assess the agreement with the 95 GeV excesses using a χ^2 -test defined as,

$$\chi_{\gamma\gamma, b\bar{b}, \tau^+\tau^-}^2 = \frac{(\mu_{\gamma\gamma, b\bar{b}, \tau^+\tau^-} - \mu_{\gamma\gamma, b\bar{b}, \tau^+\tau^-}^{\text{exp}})^2}{(\Delta\mu_{\gamma\gamma, b\bar{b}, \tau^+\tau^-}^{\text{exp}})^2}, \quad (17)$$

where $\mu_{\gamma\gamma}$, $\mu_{b\bar{b}}$ and $\mu_{\tau^+\tau^-}$ are signal strengths defined in terms of the production cross sections and decay branching ratios as follows,

$$\mu_{\gamma\gamma} = \frac{\sigma_{2\text{HDMcT}}(gg \rightarrow h_1)}{\sigma_{\text{SM}}(gg \rightarrow h_{\text{SM}})} \times \frac{\mathcal{BR}_{2\text{HDMcT}}(h_1 \rightarrow \gamma\gamma)}{\mathcal{BR}(h_{\text{SM}} \rightarrow \gamma\gamma)} \approx |c_{h_1 t\bar{t}}|^2 \times \frac{\mathcal{BR}_{2\text{HDMcT}}(h_1 \rightarrow \gamma\gamma)}{\mathcal{BR}(h_{\text{SM}} \rightarrow \gamma\gamma)}, \quad (18)$$

$$\mu_{b\bar{b}} = \frac{\sigma_{2\text{HDMcT}}(e^+e^- \rightarrow Zh_1)}{\sigma_{\text{SM}}(e^+e^- \rightarrow Zh_{\text{SM}})} \times \frac{\mathcal{BR}_{2\text{HDMcT}}(h_1 \rightarrow b\bar{b})}{\mathcal{BR}(h_{\text{SM}} \rightarrow b\bar{b})} \approx |c_{h_1 ZZ}|^2 \times \frac{\mathcal{BR}_{2\text{HDMcT}}(h_1 \rightarrow b\bar{b})}{\mathcal{BR}(h_{\text{SM}} \rightarrow b\bar{b})}, \quad (19)$$

$$\mu_{\tau^+\tau^-} = \frac{\sigma_{2\text{HDMcT}}(gg \rightarrow h_1)}{\sigma_{\text{SM}}(gg \rightarrow h_{\text{SM}})} \times \frac{\mathcal{BR}_{2\text{HDMcT}}(h_1 \rightarrow \tau^+\tau^-)}{\mathcal{BR}(h_{\text{SM}} \rightarrow \tau^+\tau^-)} \approx |c_{h_1 t\bar{t}}|^2 \times \frac{\mathcal{BR}_{2\text{HDMcT}}(h_1 \rightarrow \tau^+\tau^-)}{\mathcal{BR}(h_{\text{SM}} \rightarrow \tau^+\tau^-)} \quad (20)$$

The experimental values for $\mu_{\gamma\gamma, b\bar{b}, \tau^+\tau^-}^{\text{exp}}$ reported by CMS [20, 22] and ATLAS [23, 24, 42] are given by [¶],

$$\mu_{\gamma\gamma}^{\text{CMS}} = 0.33_{-0.12}^{+0.19} \quad (21)$$

$$\mu_{\gamma\gamma}^{\text{ATLAS}} = 0.18_{-0.10}^{+0.10} \quad (22)$$

Here σ_{SM} denotes the cross section of a hypothetical SM Higgs h_{SM} at the same mass.

An earlier analysis combined the two results in a way overlooking potential correlations. This analysis suggests a 3.1σ (local) excess at a mass of 95.4 GeV, with a signal strength [42],

$$\mu_{\gamma\gamma}^{\text{ATLAS+CMS}} = 0.24_{-0.08}^{+0.09}. \quad (23)$$

The CMS experiment also observed a similar excess in the $\tau^+\tau^-$ channel with $\mu_{\tau^+\tau^-}^{\text{CMS}} = 1.2 \pm 0.5$, corresponding to a local significance 2.6σ [25].

Also, it is worth noting that LEP reported a local excess of 2.3σ in the $b\bar{b}$ channel [12] with a signal strength,

$$\mu_{b\bar{b}}^{\text{LEP}} = 0.117 \pm 0.057. \quad (24)$$

3.1 $h_{95} \rightarrow \gamma\gamma$ and $h_{95} \rightarrow b\bar{b}$ excesses

In this section, we examine whether the 2HDMcT allowed parameter space can simultaneously account for the 95 GeV excesses observed in the two decay modes: $h_1 \rightarrow \gamma\gamma, b\bar{b}$. To this end we perform a χ^2 -test which incorporates the two contributions $\chi_{\gamma\gamma}^2$ and $\chi_{b\bar{b}}^2$, knowing that the latter depend on the model predictions for $\mu_{\gamma\gamma}$ and $\mu_{b\bar{b}}$ (see Eq.17). In order to insure that the SM-like Higgs boson h_2 aligns with the observed properties of the 125 GeV Higgs h_{125} , we also use χ_{125}^2 and impose the following condition $\Delta\chi_{125}^2 < 5.99$ ^{||} [78]. Here we impose $\Delta\chi_{125}^2 < 5.99$, with:

$$\chi_{\gamma\gamma+b\bar{b}}^2 = \chi_{\gamma\gamma}^2 + \chi_{b\bar{b}}^2 \quad (25)$$

and

$$\chi_{\text{Tot}}^2 = \chi_{\gamma\gamma}^2 + \chi_{b\bar{b}}^2 + \chi_{125}^2 \quad (26)$$

[¶]The value of $\mu_{\gamma\gamma}^{\text{ATLAS}}$ is found by normalizing the cross section reported by ATLAS [23] to its corresponding SM one [92].

^{||}The χ_{125}^2 is provided by HiggsSignals. The $\Delta\chi_{125}^2$ condition is defined as, $\Delta\chi_{125}^2 = \chi^2 - \chi_{\text{min}}^2$

In Fig. 1, we show the scatter points of the scan results in $(\mu_{\gamma\gamma}, \mu_{b\bar{b}})$ plane within 2HDMcT. The color bar shows the couplings C_{h_1ZZ} (left panel) and $C_{h_1t\bar{t}}$ (right panel) values. The regions consistent with the excesses at 1σ are represented by the dashed ellipses defined by the equation $\chi_{b\bar{b}}^2 + \chi_{\gamma\gamma}^2 = 2.30$. The black, green, and blue ellipses correspond to the χ^2 evaluated via the experimental signal strengths $\mu_{\gamma\gamma}^{\text{CMS+ATLAS}}$, $\mu_{\gamma\gamma}^{\text{ATLAS}}$, and $\mu_{\gamma\gamma}^{\text{CMS}}$, respectively. The green, red and orange stars fingerprint the points with $\min(\chi_{\gamma\gamma+b\bar{b}}^2)$, $\min(\chi_{125}^2)$ and the best fit point**, respectively. The set of generated points passing $\Delta\chi_{125}^2 < 5.99$ condition are depicted in black. We can clearly see that the 2HDMcT with Type-I Yukawa texture is capable of accounting for the two excesses simultaneously as a dense set of points occur within the 1σ ellipse. Furthermore, we also see that higher values of the couplings C_{h_1ZZ} and $C_{h_1t\bar{t}}$ correspond to larger signal strengths $\mu_{\gamma\gamma}$, $\mu_{b\bar{b}}$, as expected from Eq. 20.

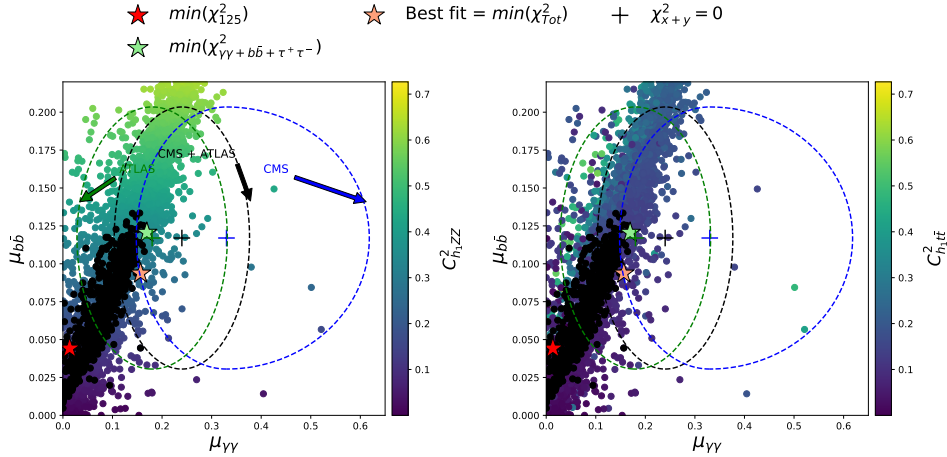


Figure 1: The scatter points in $(\mu_{b\bar{b}}, \mu_{\gamma\gamma})$ plane in the 2HDMcT. The color coding indicates the values of the couplings C_{h_1ZZ} (left panel) and $C_{h_1t\bar{t}}$ (right panel). Confidence levels of 1σ with respect to $\chi_{\gamma\gamma+b\bar{b}}^2$ are illustrated by dashed ellipses. Black, green and blue represent the predictions for $\mu_{\gamma\gamma}$ using the CMS+ATLAS, ATLAS and CMS data, respectively. Only the points in black satisfy the condition $\Delta\chi_{125}^2 < 5.99$. The green, red and orange stars indicate the points with $\min(\chi_{\gamma\gamma+b\bar{b}}^2)$, $\min(\chi_{125}^2)$ and the best fit point, respectively.

Similarly Fig. 2 displays scattered points in the $(\mu_{\gamma\gamma}, \mu_{b\bar{b}})$ plane. The color bar displays the values of $\cos\alpha_1$ (left), $\tan\beta$ (middle), and $\Delta\chi_{125}^2$ (right). For a given $\mu_{b\bar{b}}$, the largest $\mu_{\gamma\gamma}$ corresponds to largest $\tan\beta$. In contrast, for a fixed $\mu_{\gamma\gamma}$, we get sizable $\mu_{b\bar{b}}$ when $\tan\beta$ is smaller. A similar pattern occurs with $\cos\alpha_1$, except that most allowed points originate from relatively large values of $\cos\alpha_1$. Additionally, we can also see that $\mu_{\gamma\gamma}$ increases when $\Delta\chi_{125}^2$ gets large, corresponding to generating points representing most accurately the excesses. Consequently, the point with $\min(\chi_{125}^2)$, signaled by a red star, lies outside the 1σ ellipse. In order to probe how the excesses affects the parameters $\cos\alpha_1$ and $\tan\beta$, we display in Fig. 3 $\chi_{\gamma\gamma+b\bar{b}}^2$ versus $\cos\alpha_1$, where the color coding indicates $\tan\beta$ values. We can readily deduce that simultaneously describing both excesses at the 1σ confidence level requires these parameters to lie within the following intervals :

$$0.83 \leq \cos\alpha_1 \leq 0.96, \quad 4 \leq \tan\beta \leq 30 \quad (27)$$

**It is worth to recall that the best-fit point corresponds to the minimum value of χ_{Tot}^2 .

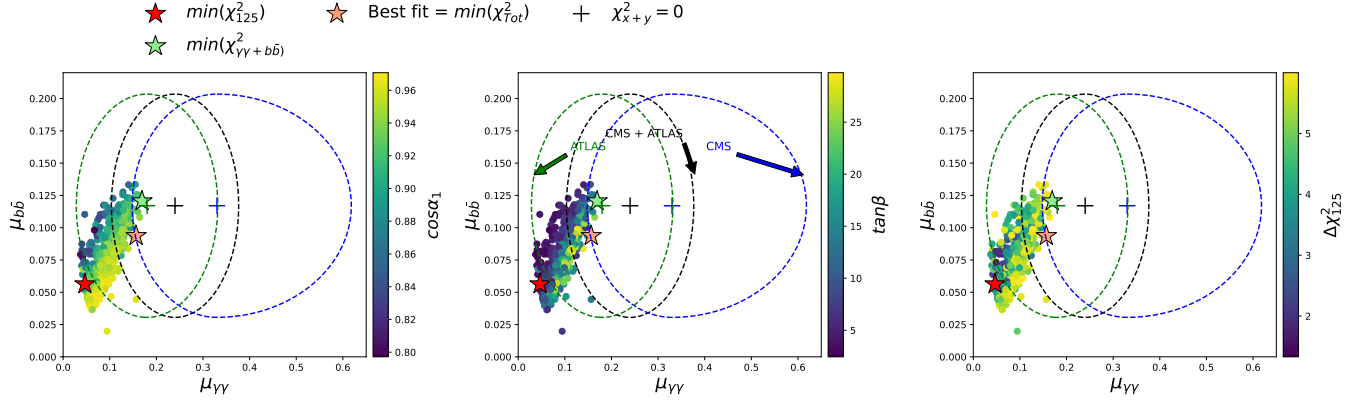


Figure 2: As in Fig.1 the scatter points in $(\mu_{\gamma\gamma}, \mu_{b\bar{b}})$ plane in the 2HDMcT are presented. The color coding indicates the values of $\cos \alpha_1$ (left), $\tan \beta$ (middle) and $\Delta\chi^2_{125}$ (right). The green, red and orange stars marking the points with $\min(\chi^2_{\gamma\gamma+b\bar{b}})$, $\min(\chi^2_{125})$ and the best fit point, respectively.

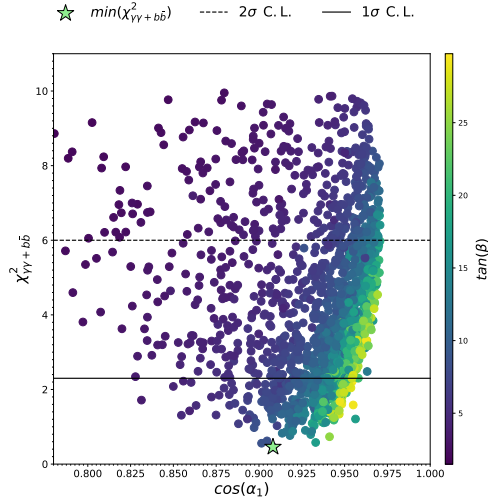


Figure 3: Scattered points in the plane $(\cos \alpha_1, \chi^2_{\gamma\gamma+b\bar{b}})$. The color bar indicates the value of $\tan \beta$. The horizontal solid and dashed lines represent the 1σ and 2σ regions, respectively. The green star indicates the point with $\min(\chi^2_{\gamma\gamma+b\bar{b}})$.

3.2 $h_{95} \rightarrow \gamma\gamma$, $h_{95} \rightarrow b\bar{b}$ and $h_{95} \rightarrow \tau^+\tau^-$ excesses

Besides the $\gamma\gamma$ excess, the CMS experiment has also reported an excess in the $\tau^+\tau^-$ decay channel with a local significance of 2.6σ [25]. Here, we explore whether the 2HDMcT model is able to provide a unified explanation to the three observed excesses. To do so, we also incorporate the contribution from $\chi_{\tau^+\tau^-}^2$ and define the following χ^2 tests:

$$\chi_{\gamma\gamma+b\bar{b}+\tau^+\tau^-}^2 = \chi_{\gamma\gamma}^2 + \chi_{b\bar{b}}^2 + \chi_{\tau^+\tau^-}^2 \quad (28)$$

and

$$\chi_{Tot}^2 = \chi_{\gamma\gamma}^2 + \chi_{b\bar{b}}^2 + \chi_{\tau^+\tau^-}^2 + \chi_{125}^2 \quad (29)$$

In Fig. 4, the scattered points in the signal strengths $(\mu_{\gamma\gamma}, \mu_{b\bar{b}})$ (left), $(\mu_{\gamma\gamma}, \mu_{\tau^+\tau^-})$ (middle)

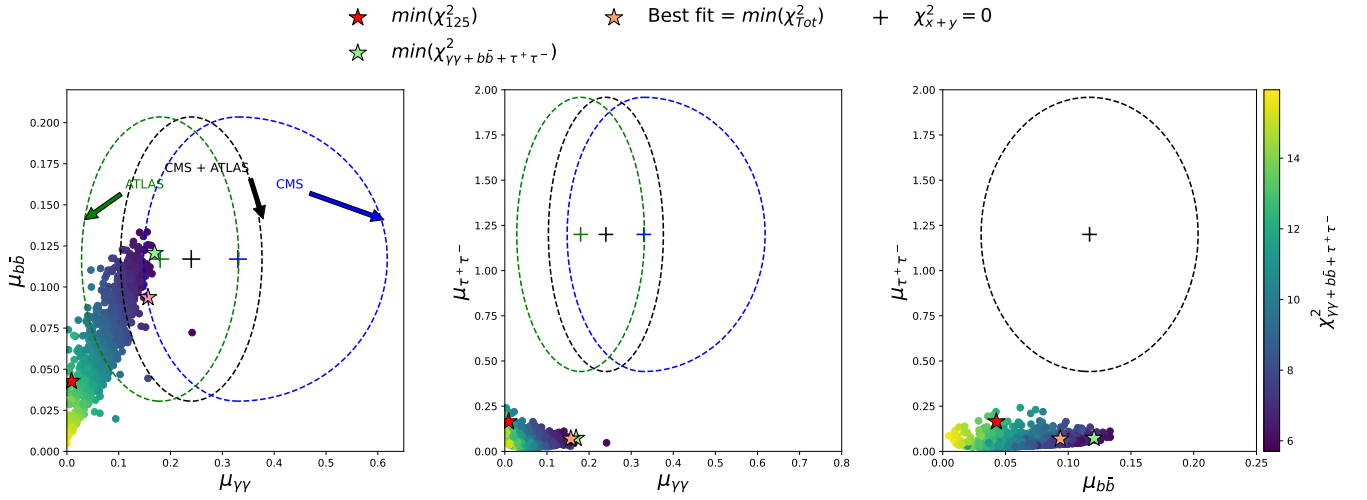


Figure 4: The colour map of $\chi_{\gamma\gamma+\tau^+\tau^-+b\bar{b}}^2$ in the $(\mu_{\gamma\gamma}, \mu_{b\bar{b}})$, $(\mu_{\gamma\gamma}, \mu_{\tau^+\tau^-})$ and $(\mu_{b\bar{b}}, \mu_{\tau^+\tau^-})$ planes of the signal strength parameters for 2HDMcT parameter space under study. The ellipses define the regions consistent with the excess at 1σ C.L. The black, green, and blue ellipses correspond to the χ^2 values calculated using the experimental signal strengths $\mu_{\gamma\gamma}^{\text{CMS+ATLAS}}$, $\mu_{\gamma\gamma}^{\text{ATLAS}}$, and $\mu_{\gamma\gamma}^{\text{CMS}}$, respectively. The green, red and orange stars marking the points with $\min(\chi_{\gamma\gamma+b\bar{b}+\tau^+\tau^-}^2)$, $\min(\chi_{125}^2)$ and the best fit point, respectively.

and $(\mu_{b\bar{b}}, \mu_{\tau^+\tau^-})$ (right) planes are presented. The dashed ellipses indicate regions consistent with the two-dimensional 1σ excess in (μ_x, μ_y) , described by the equation $\chi_x^2 + \chi_y^2 = 2.30$, where the subscripts x and y represent each possible pairing of the three signal channels ($\gamma\gamma$, $\tau^+\tau^-$, and $b\bar{b}$). The black, green, and blue ellipses show the χ^2 values computed from the experimental signal strengths $\mu_{\gamma\gamma}^{\text{CMS+ATLAS}}$, $\mu_{\gamma\gamma}^{\text{ATLAS}}$, and $\mu_{\gamma\gamma}^{\text{CMS}}$, respectively. The green, red and orange stars marking the points with $\min(\chi_{\gamma\gamma+b\bar{b}}^2)$, $\min(\chi_{125}^2)$ and the best fit point, respectively. The color coding indicates the value of $\chi_{\gamma\gamma+\tau^+\tau^-+b\bar{b}}^2$. We can clearly see from the left panel that many points lie solely within the 1σ C.L. ellipse for the $(\mu_{b\bar{b}}, \mu_{\gamma\gamma})$ pair, however no point does so for the other two pairs since it is quite difficult to achieve larger values for the two pairs simultaneously. Consequently the model cannot account for all three excesses at 1σ C.L. simultaneously. The point indicated by the green star corresponding to $\min(\chi_{\gamma\gamma+\tau^+\tau^-+b\bar{b}}^2)$ has a value of 5.7, corresponding to about 1.4σ C.L. for three degrees of freedom. So by assuming that the observed signal originates only

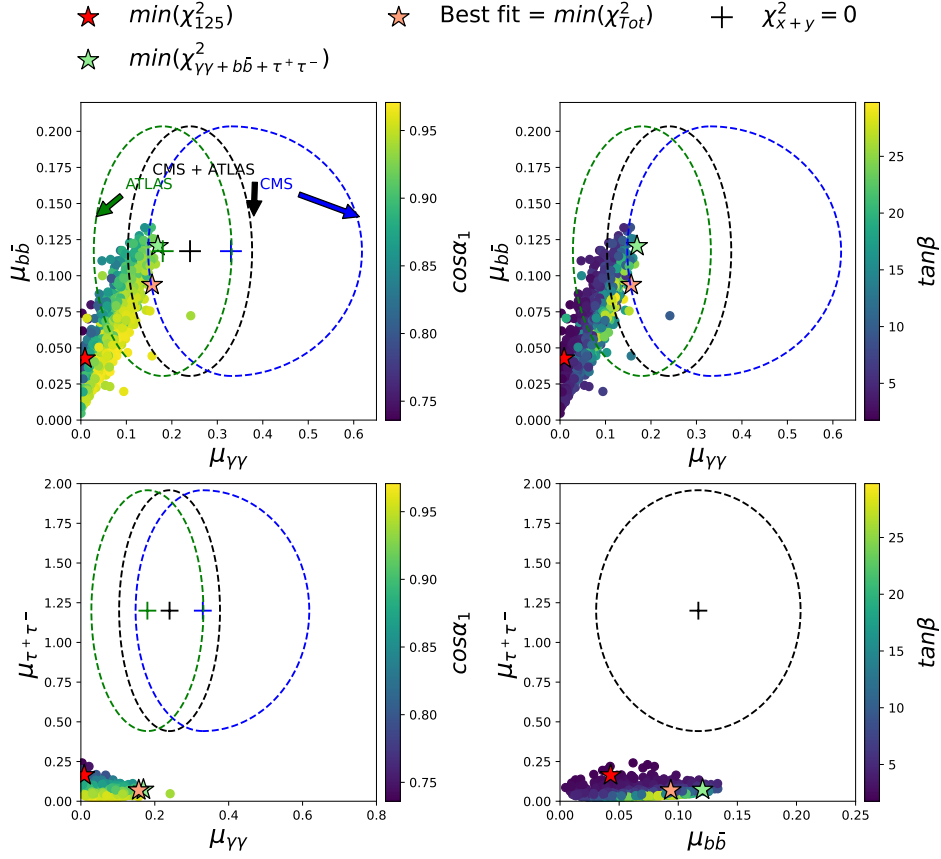


Figure 5: Just as in Fig. 4 the scatter points in $(\mu_{\gamma\gamma}, \mu_{b\bar{b}})$ (upper panels) and $(\mu_{\gamma\gamma}, \mu_{\tau^+\tau^-}), (\mu_{b\bar{b}}, \mu_{\tau^+\tau^-})$ (lower panels) planes in the 2HDMcT are presented. The color coding indicates the values of $\cos \alpha_1$ (left), $\tan \beta$ (right). The green, red and orange stars marking the points with $\min(\chi^2_{\gamma\gamma+b\bar{b}+\tau^+\tau^-})$, $\min(\chi^2_{125})$ and the best fit point, respectively.

from the CP-even Higgs h_1 , the 2HDMcT can explain the observed excess across all three channels simultaneously at about 1.4σ C.L. at best

Similarly in Fig. 5, we plotted the allowed points in $(\mu_{\gamma\gamma}, \mu_{b\bar{b}})$ (upper panels) and $(\mu_{\gamma\gamma}, \mu_{\tau^+\tau^-}), (\mu_{b\bar{b}}, \mu_{\tau^+\tau^-})$ (lower panels) planes. The color coding indicates the values of $\cos \alpha_1$ (left panels) and $\tan \beta$ (right panel). In the upper panels of Fig. 5, we observe a similar dependence of $\mu_{\gamma\gamma}$ and $\mu_{b\bar{b}}$ on $\tan \beta$ and $\cos \alpha_1$ as seen in Fig. 2. Specifically, $\mu_{\gamma\gamma}$ gets large for sizable values of $\tan \beta$ and $\cos \alpha_1$. In contrast, the lower panels of Fig. 5 show that the points with smallest $\tan \beta$ and $\cos \alpha_1$ produce larger $\mu_{\tau^+\tau^-}$. Consequently, our analysis show that it is not possible to achieve large values for both $\mu_{\gamma\gamma}$ and $\mu_{\tau^+\tau^-}$ simultaneously, thereby preventing the simultaneous 1σ accounting for both excesses. In the subsequent section, we will investigate whether a superposition of the CP-even and CP-odd states with a nearly degenerate mass can account for all the observed excesses.

3.3 The Superposition Solution

In the previous sections we have shown that the 2HDMcT can well describe the $\gamma\gamma$ and $b\bar{b}$ excesses simultaneously. On the other hand, we have seen that the model fails to account for the three excesses simultaneously, namely, $\gamma\gamma$, $b\bar{b}$ and $\tau^+\tau^-$ at 1σ C.L. A legitimate question arise, whether these excesses are a manifest of the superposition of two or more resonances at the comparable mass.

Here, we will explore this scenario and see if the model can explain all the excesses simultaneously. To do this, we conduct a combined analysis of the CP-even (h_1) and CP-odd (A_1) resonances^{††}. In the CP-conserving scenario the pseudoscalar state A_1 cannot contribute to $\mu_{b\bar{b}}$ given that the coupling $C_{A_1 ZZ}$ is forbidden at tree level. On the other hand the state A_1 do contribute to both $\mu_{\gamma\gamma}$ and $\mu_{\tau^+\tau^-}$. In this case the combined contributions to the signal strengths for the three resonances $\gamma\gamma$, $b\bar{b}$ and $\tau^+\tau^-$, reads as follows:

$$\begin{aligned}\mu_{\gamma\gamma}(h_1 + A_1) &= \mu_{\gamma\gamma}(h_1) + \mu_{\gamma\gamma}(A_1), \\ \mu_{\tau^+\tau^-}(h_1 + A_1) &= \mu_{\tau^+\tau^-}(h_1) + \mu_{\tau^+\tau^-}(A_1), \\ \mu_{b\bar{b}}(h_1 + A_1) &= \mu_{b\bar{b}}(h_1),\end{aligned}\tag{30}$$

††

Since we assumed CP conservation in the 2HDMcT model, there is no interference between the h_1 and A_1 states. In a similar pattern to Fig. 4, and taking contributions from both states h_1 and A_1 as defined in Eq. 30, we display the scattered points in the signal strengths ($\mu_{\gamma\gamma}$, $\mu_{b\bar{b}}$) (left), ($\mu_{\gamma\gamma}$, $\mu_{\tau^+\tau^-}$) (middle) and ($\mu_{b\bar{b}}$, $\mu_{\tau^+\tau^-}$) (right) planes. We clearly see that a dense set of points lies within the 1σ level in both ($\mu_{\gamma\gamma}$, $\mu_{b\bar{b}}$), ($\mu_{\gamma\gamma}$, $\mu_{\tau^+\tau^-}$) planes and a few in the ($\mu_{b\bar{b}}$, $\mu_{\tau^+\tau^-}$) plane, but in all cases the point with $\min(\chi^2_{\gamma\gamma+b\bar{b}+\tau^+\tau^-})$, indicated by the green star lies within the 1σ ellipse. This proves that the 2HDMcT is able to account for the observed excesses at 1σ C.L when we consider the superposition of ($h_1 + A_1$) states. The $\min(\chi^2_{\gamma\gamma+\tau^+\tau^-+b\bar{b}}) = 2.25$, corresponding to about 0.64σ C.L, is the model's best description of the three-dimensional excesses. This point is displayed in Table 4. The generated points explaining the three excesses at 1σ ($\chi^2 \leq 3.53$) are marked in black in the figures.

For a direct comparison with the experimental data, we superimpose our predictions for $\mu_{\gamma\gamma}$ onto the CMS 13 TeV low-mass $\gamma\gamma$ analysis data in Fig. 7. The expected and observed cross-section limits obtained by CMS (black) and ATLAS (red) are displayed by dashed and solid lines, respectively. The green and yellow bands correspond to the 1σ and 2σ uncertainty intervals, respectively. The error bar in yellow indicates the value of $\mu_{\gamma\gamma}^{CMS+ATLAS}$, along with its respective uncertainty. One can readily see that the 2HDMcT can well accommodate the combined $\mu_{\gamma\gamma}$ observed excess.

In order to see how the excesses impact the parameters $\cos\alpha_1$ and $\tan\beta$ and compare with the results shown in Fig. 3, we display in Fig. 8, $\chi^2_{\gamma\gamma+\tau^+\tau^-+b\bar{b}}$ with parameter scans as a function of $\cos\alpha_1$. The color bar indicates $\tan\beta$ values. The horizontal solid and dashed lines represent the 1σ and 2σ regions respectively. We can clearly see that describing simultaneously the three excesses at 1σ C.L is possible, imposing constraints on the allowed ranges of $\tan\beta$ and $\cos\alpha_1$. In

^{††}The input parameters are the same as in 16 plus $93\text{ GeV} \leq m_{A_1} \leq 97\text{ GeV}$.

^{‡‡} $\mu_{b\bar{b}}(A_1) = 0$.

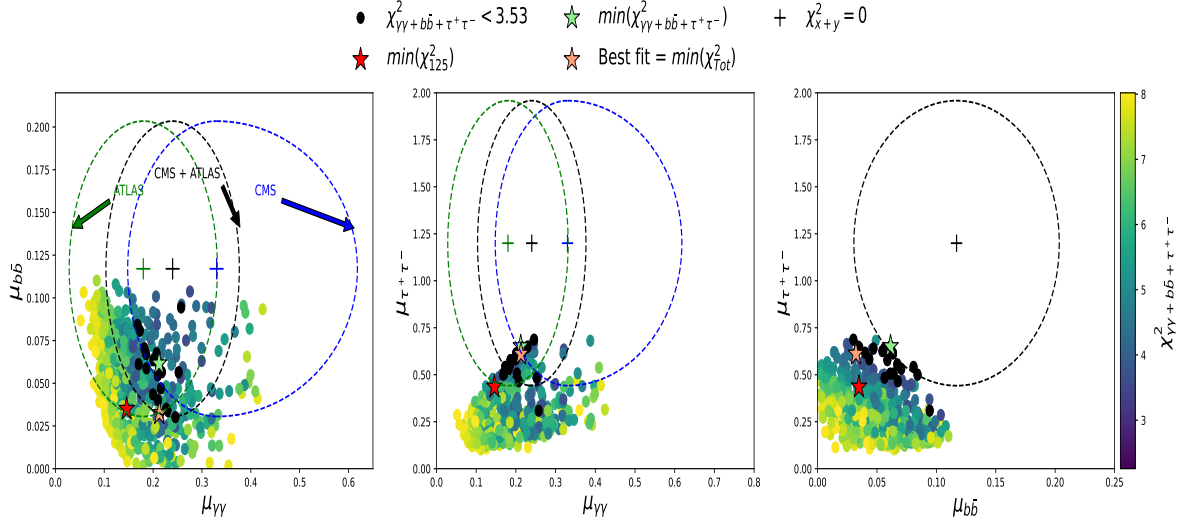


Figure 6: The scattered points in the plane of $(\mu(h_1 + A_1)_{\gamma\gamma}, \mu(h_1 + A_1)_{\tau^+\tau^-})$ within the 2HDMcT. The green, red and orange stars marking the points with $\min(\chi^2_{\gamma\gamma+b\bar{b}+\tau^+\tau^-})$, $\min(\chi^2_{125})$ and the best fit point, respectively. The black points feature $\chi^2_{\gamma\gamma+\tau^+\tau^-+b\bar{b}} \leq 3.53$ and describe the excesses at the level of 1σ or better.

particular, these parameters lie within a drastically reduced intervals compared to those found in Sec. 3.1, namely :

$$0.78 \leq \cos \alpha_1 \leq 0.86, \quad 2 \leq \tan \beta \leq 5 \quad (31)$$

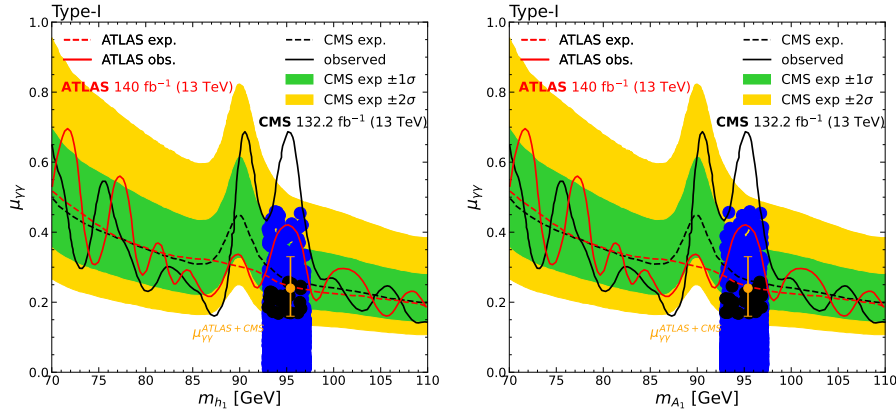


Figure 7: Scattered points in the $(m_{h_1}, \mu_{\gamma\gamma})$ and $(m_{A_1}, \mu_{\gamma\gamma})$ planes. The dashed and solid lines represent the expected and observed cross-section limits obtained by CMS and ATLAS, respectively. CMS is depicted in black, while ATLAS is shown in red. The green and yellow bands represent the 1σ and 2σ uncertainty intervals, respectively. The yellow error bar indicates the values of $\mu_{\gamma\gamma}^{CMS+ATLAS}$, along with its uncertainty. The black points feature $\chi^2_{\gamma\gamma+\tau^+\tau^-+b\bar{b}} \leq 3.53$ and describe the excesses at the level of 1σ or better, whereas the blue points represent $\chi^2_{\gamma\gamma+\tau^+\tau^-+b\bar{b}} > 3.53$.

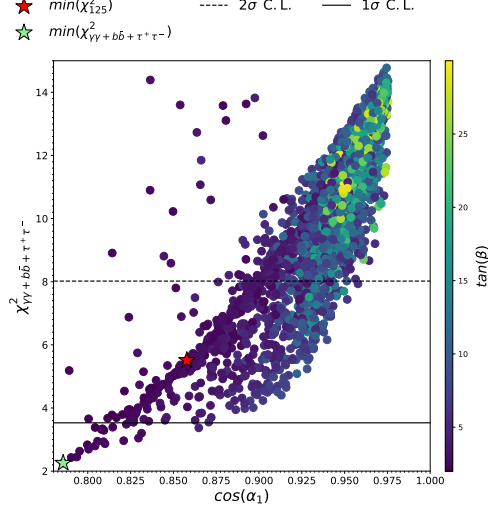


Figure 8: Scattered points in the plane of $(\cos \alpha_1, \chi^2_{\gamma\gamma+\tau^+\tau^-+b\bar{b}})$. The color bar indicates the value of $\tan\beta$. The horizontal solid and dashed lines represents the 1σ and 2σ regions respectively.

Parameters	m_{h_1}	m_{h_2}	λ_1	λ_3	λ_4	λ_6	λ_7	λ_8	λ_9	$\bar{\lambda}_8$	$\bar{\lambda}_9$	$\tan\beta$	α_1	α_2	α_3	v_t	μ_1
	95.56	125.09	0.13	0.43	-0.13	2.99	4.06	1.35	2.63	2.64	-1.27	2.25	-0.66	-0.08	-0.02	1	-43.57
Signal strengths	$\mu_{\gamma\gamma}(h_1)$	$\mu_{\gamma\gamma}(A_1)$	$\mu_{\gamma\gamma}(h_1 + A_1)$		$\mu_{\tau^+\tau^-}(h_1)$		$\mu_{\tau^+\tau^-}(A_1)$	$\mu_{\tau^+\tau^-}(h_1 + A_1)$		$\mu_{b\bar{b}}(h_1)$							
	0.02	0.19	0.21		0.45		0.19	0.65		0.062							

Table 4: Description of our point corresponding to $\min(\chi^2_{\gamma\gamma+\tau^+\tau^-+b\bar{b}})$.

4 Conclusions

In the present paper, driven by emerging observations of a scalar resonance with an invariant mass distribution about 95 GeV, we have studied whether the 2HDM augmented with a complex scalar triplet, can account for the reported excesses. Our analysis and results satisfied a full set of constraints on the model parameter space, with the h_2 Higgs predicted by the model spectrum mimics the observed h_{125} at the LHC. First, we analyzed the two excesses in the $\gamma\gamma$ and $b\bar{b}$ decay channels. We showed that the 2HDMcT model with the Type-I Yukawa texture can simultaneously accommodate these two excesses. Then, we remarkably found that the three excesses in $\gamma\gamma$, $b\bar{b}$ and $\tau^+\tau^-$ channels can well be explained simultaneously, reaching a 0.64σ C.L. when the CP-odd Higgs boson A_1 is nearly mass degenerate and superposed to the light Higgs h_1 . In the near future, the Run 3 data from ATLAS and CMS around 95 GeV will help shed further light and clarify whether the observed excesses are an early indication of a new particle discovery and new physics beyond the Standard Model.

APPENDIX : The Higgs Decay to Two Photons

In addition to the contributions from Standard Model particles, the loop-mediated decay of a scalar particle also receives extra contributions from the charged Higgs particles. In the context of the Two Higgs Doublet Model with a Triplet (2HDMcT), which includes an additional Triplet field, the particle spectrum predicts the existence of three pairs of charged particles. This is two more than what the conventional Two Higgs Doublet Model (2HDM) predicts. The decay width for $h_1 \rightarrow \gamma\gamma$ in 2HDMcT is given by,

$$\Gamma(h_1 \rightarrow \gamma\gamma) = \frac{G_\mu \alpha^2 M_{h_1}^3}{128 \sqrt{2} \pi^3} \left| \sum_{f=l,q} N_c Q_f^2 g_{h_1 f f} A_{1/2}^{h_1}(\tau_f) + g_{h_1 V V} A_1^{h_1}(\tau_W) + \sum_{i=1,2} \frac{M_W^2 \lambda_{h_1 H_i^+ H_i^-}}{2 c_W^2 M_{H_i^\pm}^2} A_0^{h_1}(\tau_{H_i^\pm}) + \frac{2 M_W^2 \lambda_{h_1 H^{++} H^{--}}}{c_W^2 M_{H^{\pm\pm}}^2} A_0^{h_1}(\tau_{H^{\pm\pm}}) \right|^2 \quad (32)$$

The reduced couplings $g_{h_1 f f}$ and $g_{h_1 V V}$ of the Higgs bosons to fermions and W bosons are given in Tab. 1 and Tab. 2, while the trilinear $\lambda_{h_1 H_i^+ H_i^-}$ and $\lambda_{h_1 H^\pm H^\pm}$ couplings to charged Higgs bosons are given by [93],

$$\begin{aligned} A_{1/2}^{h_1}(\tau) &= 2[\tau + (\tau - 1)f(\tau)] \tau^{-2} \\ A_1^{h_1}(\tau) &= -[2\tau^2 + 3\tau + 3(2\tau - 1)f(\tau)] \tau^{-2} \\ A_0^{h_1}(\tau) &= -[\tau - f(\tau)] \tau^{-2} \end{aligned} \quad (33)$$

The scaling variables are defined as $\tau_i = M_\Phi^2/4M_i^2$, where M_i represents the loop mass. In this context, M_i encompasses all Standard Model charged particles as well as the Charged Higgs bosons predicted by the model, which provide additional contributions to the process.

$$\begin{aligned} \bar{\lambda}_{h_1 H_1^\pm H_1^\pm} &= \frac{s_w}{2em_w} (2\mathcal{C}_{21}^2 (\lambda_6 \mathcal{E}_{13} v_\Delta + \lambda_1 v_1 \mathcal{E}_{11} + \lambda_3 v_2 \mathcal{E}_{12}) \\ &+ 2\mathcal{C}_{22}^2 (\lambda_7 \mathcal{E}_{13} v_\Delta + \lambda_2 v_2 \mathcal{E}_{12} + \lambda_3 v_1 \mathcal{E}_{11}) \\ &+ \mathcal{C}_{23}^2 (2\mathcal{E}_{13} (2\bar{\lambda}_8 + \bar{\lambda}_9) v_\Delta + (2\lambda_6 + \lambda_8) v_1 \mathcal{E}_{11} + (2\lambda_7 + \lambda_9) v_2 \mathcal{E}_{12}) \\ &+ \mathcal{C}_{22} \mathcal{C}_{23} (\sqrt{2} \lambda_9 \mathcal{E}_{12} v_\Delta + \sqrt{2} \lambda_9 v_2 \mathcal{E}_{13} - 4\mu_2 \mathcal{E}_{12} - 2\mu_3 \mathcal{E}_{11}) \\ &+ \mathcal{C}_{21} (\mathcal{C}_{23} (\sqrt{2} \lambda_8 \mathcal{E}_{11} v_\Delta + \sqrt{2} \lambda_8 v_1 \mathcal{E}_{13} - 4\mu_1 \mathcal{E}_{11} - 2\mu_3 \mathcal{E}_{12}) \\ &+ 2\mathcal{C}_{22} (\lambda_4 + \lambda_5) (v_2 \mathcal{E}_{11} + v_1 \mathcal{E}_{12})) \end{aligned} \quad (34)$$

$$\begin{aligned} \bar{\lambda}_{h_1 H_2^\pm H_2^\pm} &= \frac{s_w}{2em_w} (2\mathcal{C}_{31}^2 (\lambda_6 \mathcal{E}_{13} v_\Delta + \lambda_1 v_1 \mathcal{E}_{11} + \lambda_3 v_2 \mathcal{E}_{12}) \\ &+ 2\mathcal{C}_{32}^2 (\lambda_7 \mathcal{E}_{13} v_\Delta + \lambda_2 v_2 \mathcal{E}_{12} + \lambda_3 v_1 \mathcal{E}_{11}) \\ &+ \mathcal{C}_{33}^2 (2\mathcal{E}_{13} (2\bar{\lambda}_8 + \bar{\lambda}_9) v_\Delta + (2\lambda_6 + \lambda_8) v_1 \mathcal{E}_{11} + (2\lambda_7 + \lambda_9) v_2 \mathcal{E}_{12}) \\ &+ \mathcal{C}_{32} \mathcal{C}_{33} (\sqrt{2} \lambda_9 \mathcal{E}_{12} v_\Delta + \sqrt{2} \lambda_9 v_2 \mathcal{E}_{13} - 4\mu_2 \mathcal{E}_{12} - 2\mu_3 \mathcal{E}_{11}) \\ &+ \mathcal{C}_{31} (\mathcal{C}_{33} (\sqrt{2} \lambda_8 \mathcal{E}_{11} v_\Delta + \sqrt{2} \lambda_8 v_1 \mathcal{E}_{13} - 4\mu_1 \mathcal{E}_{11} - 2\mu_3 \mathcal{E}_{12}) \\ &+ 2\mathcal{C}_{32} (\lambda_4 + \lambda_5) (v_2 \mathcal{E}_{11} + v_1 \mathcal{E}_{12})) \end{aligned} \quad (35)$$

$$\bar{\lambda}_{h_1 H^{\pm\pm} H^{\pm\pm}} = \frac{s_w}{em_w} (2\bar{\lambda}_8 \mathcal{E}_{13} v_\Delta + \lambda_6 v_1 \mathcal{E}_{11} + \lambda_7 v_2 \mathcal{E}_{12}) \quad (36)$$

5 Acknowledgments

The authors would like to thank CNRST/HPC-MARWAN for technical support.

References

- [1] **ATLAS** collaboration, G. Aad et al., *Observation of a new particle in the search for the Standard Model Higgs boson with the ATLAS detector at the LHC*, *Phys. Lett. B* **716** (2012) 1–29, [[1207.7214](#)].
- [2] **CMS** collaboration, S. Chatrchyan et al., *Observation of a New Boson at a Mass of 125 GeV with the CMS Experiment at the LHC*, *Phys. Lett. B* **716** (2012) 30–61, [[1207.7235](#)].
- [3] **ATLAS, CMS** collaboration, G. Aad et al., *Measurements of the Higgs boson production and decay rates and constraints on its couplings from a combined ATLAS and CMS analysis of the LHC pp collision data at $\sqrt{s} = 7$ and 8 TeV*, *JHEP* **08** (2016) 045, [[1606.02266](#)].
- [4] **CMS** collaboration, A. Tumasyan et al., *A portrait of the Higgs boson by the CMS experiment ten years after the discovery.*, *Nature* **607** (2022) 60–68, [[2207.00043](#)].
- [5] **ATLAS** collaboration, G. Aad et al., *A detailed map of Higgs boson interactions by the ATLAS experiment ten years after the discovery*, *Nature* **607** (2022) 52–59, [[2207.00092](#)]. [Erratum: *Nature* 612, E24 (2022)].
- [6] F. Zwicky, *Die Rotverschiebung von extragalaktischen Nebeln*, *Helv. Phys. Acta* **6** (1933) 110–127.
- [7] V. C. Rubin and W. K. Ford, Jr., *Rotation of the Andromeda Nebula from a Spectroscopic Survey of Emission Regions*, *Astrophys. J.* **159** (1970) 379–403.
- [8] M. J. G. Veltman, *The Infrared - Ultraviolet Connection*, *Acta Phys. Polon. B* **12** (1981) 437.
- [9] T. Kajita, *Nobel lecture: Discovery of atmospheric neutrino oscillations*, *Rev. Mod. Phys.* **88** (Jul, 2016) 030501.
- [10] A. B. McDonald, *Nobel lecture: The sudbury neutrino observatory: Observation of flavor change for solar neutrinos*, *Rev. Mod. Phys.* **88** (Jul, 2016) 030502.
- [11] **OPAL** collaboration, G. Abbiendi et al., *Decay mode independent searches for new scalar bosons with the OPAL detector at LEP*, *Eur. Phys. J. C* **27** (2003) 311–329, [[hep-ex/0206022](#)].
- [12] **LEP Working Group for Higgs boson searches, ALEPH, DELPHI, L3, OPAL** collaboration, R. Barate et al., *Search for the standard model Higgs boson at LEP*, *Phys. Lett. B* **565** (2003) 61–75, [[hep-ex/0306033](#)].
- [13] **ALEPH, DELPHI, L3, OPAL, LEP Working Group for Higgs Boson Searches** collaboration, S. Schael et al., *Search for neutral MSSM Higgs bosons at LEP*, *Eur. Phys. J. C* **47** (2006) 547–587, [[hep-ex/0602042](#)].
- [14] **CDF, D0** collaboration, *Updated Combination of CDF and D0 Searches for Standard Model Higgs Boson Production with up to 10.0 fb⁻¹ of Data*, 7, 2012. [1207.0449](#).
- [15] **CMS** collaboration, *Search for new resonances in the diphoton final state in the mass range between 80 and 115 GeV in pp collisions at $\sqrt{s} = 8$ TeV*, .
- [16] **CMS** collaboration, A. M. Sirunyan et al., *Search for a standard model-like Higgs boson in the mass range between 70 and 110 GeV in the diphoton final state in proton-proton collisions at $\sqrt{s} = 8$ and 13 TeV*, *Phys. Lett. B* **793** (2019) 320–347, [[1811.08459](#)].
- [17] **CMS** collaboration, *Searches for additional Higgs bosons and vector leptoquarks in $\tau\tau$ final states in proton-proton collisions at $\sqrt{s} = 13$ TeV*, , CERN, Geneva, 2022.

- [18] **CMS** collaboration, *Search for new resonances in the diphoton final state in the mass range between 70 and 110 GeV in pp collisions at $\sqrt{s} = 8$ and 13 TeV*, , CERN, Geneva, 2017.
- [19] **CMS** collaboration, A. M. Sirunyan et al., *Search for additional neutral MSSM Higgs bosons in the $\tau\tau$ final state in proton-proton collisions at $\sqrt{s} = 13$ TeV*, *JHEP* **09** (2018) 007, [[1803.06553](#)].
- [20] **CMS** collaboration, *Search for a standard model-like Higgs boson in the mass range between 70 and 110 GeV in the diphoton final state in proton-proton collisions at $\sqrt{s} = 13$ TeV*, , CERN, Geneva, 2023.
- [21] **ATLAS** collaboration, *Search for resonances in the 65 to 110 GeV diphoton invariant mass range using 80 fb⁻¹ of pp collisions collected at $\sqrt{s} = 13$ TeV with the ATLAS detector*, , CERN, Geneva, 2018.
- [22] **CMS** collaboration, A. Hayrapetyan et al., *Search for a standard model-like Higgs boson in the mass range between 70 and 110 GeV in the diphoton final state in proton-proton collisions at $\sqrt{s} = 13$ TeV*, [2405.18149](#).
- [23] **ATLAS** collaboration, G. Aad et al., *Search for diphoton resonances in the 66 to 110 GeV mass range using pp collisions at $\sqrt{s} = 13$ TeV with the ATLAS detector*, [2407.07546](#).
- [24] **ATLAS** collaboration, *Search for diphoton resonances in the 66 to 110 GeV mass range using 140 fb⁻¹ of 13 TeV pp collisions collected with the ATLAS detector*, , CERN, Geneva, 2023.
- [25] **CMS** collaboration, A. Tumasyan et al., *Searches for additional Higgs bosons and for vector leptoquarks in $\tau\tau$ final states in proton-proton collisions at $\sqrt{s} = 13$ TeV*, *JHEP* **07** (2023) 073, [[2208.02717](#)].
- [26] J. Cao, X. Guo, Y. He, P. Wu and Y. Zhang, *Diphoton signal of the light Higgs boson in natural NMSSM*, *Phys. Rev. D* **95** (2017) 116001, [[1612.08522](#)].
- [27] G. Cacciapaglia, A. Deandrea, S. Gascon-Shotkin, S. Le Corre, M. Lethuillier and J. Tao, *Search for a lighter Higgs boson in Two Higgs Doublet Models*, *JHEP* **12** (2016) 068, [[1607.08653](#)].
- [28] A. Crivellin, J. Heeck and D. Müller, *Large $h \rightarrow bs$ in generic two-Higgs-doublet models*, *Phys. Rev. D* **97** (2018) 035008, [[1710.04663](#)].
- [29] T. Biekötter, M. Chakraborti and S. Heinemeyer, *A 96 GeV Higgs boson in the N2HDM*, *Eur. Phys. J. C* **80** (2020) 2, [[1903.11661](#)].
- [30] J. M. Cline and T. Toma, *Pseudo-Goldstone dark matter confronts cosmic ray and collider anomalies*, *Phys. Rev. D* **100** (2019) 035023, [[1906.02175](#)].
- [31] J. Cao, X. Jia, Y. Yue, H. Zhou and P. Zhu, *96 GeV diphoton excess in seesaw extensions of the natural NMSSM*, *Phys. Rev. D* **101** (2020) 055008, [[1908.07206](#)].
- [32] A. A. Abdelalim, B. Das, S. Khalil and S. Moretti, *Di-photon decay of a light Higgs state in the BLSSM*, *Nucl. Phys. B* **985** (2022) 116013, [[2012.04952](#)].
- [33] T. Biekötter and M. O. Olea-Romacho, *Reconciling Higgs physics and pseudo-Nambu-Goldstone dark matter in the S2HDM using a genetic algorithm*, *JHEP* **10** (2021) 215, [[2108.10864](#)].
- [34] S. Heinemeyer, C. Li, F. Lika, G. Moortgat-Pick and S. Paasch, *Phenomenology of a 96 GeV Higgs boson in the 2HDM with an additional singlet*, *Phys. Rev. D* **106** (2022) 075003, [[2112.11958](#)].
- [35] T. Biekötter, A. Grohsjean, S. Heinemeyer, C. Schwanenberger and G. Weiglein, *Possible indications for new Higgs bosons in the reach of the LHC: N2HDM and NMSSM interpretations*, *Eur. Phys. J. C* **82** (2022) 178, [[2109.01128](#)].
- [36] T. Biekötter, S. Heinemeyer and G. Weiglein, *Excesses in the low-mass Higgs-boson search and the W-boson mass measurement*, *Eur. Phys. J. C* **83** (2023) 450, [[2204.05975](#)].

- [37] S. Iguro, T. Kitahara and Y. Omura, *Scrutinizing the 95–100 GeV di-tau excess in the top associated process*, *Eur. Phys. J. C* **82** (2022) 1053, [[2205.03187](#)].
- [38] W. Li, H. Qiao and J. Zhu, *Light Higgs boson in the NMSSM confronted with the CMS di-photon and di-tau excesses**, *Chin. Phys. C* **47** (2023) 123102, [[2212.11739](#)].
- [39] T. Biekötter, S. Heinemeyer and G. Weiglein, *Mounting evidence for a 95 GeV Higgs boson*, *JHEP* **08** (2022) 201, [[2203.13180](#)].
- [40] T. Biekötter, S. Heinemeyer and G. Weiglein, *The CMS di-photon excess at 95 GeV in view of the LHC Run 2 results*, *Phys. Lett. B* **846** (2023) 138217, [[2303.12018](#)].
- [41] D. Azevedo, T. Biekötter and P. M. Ferreira, *2HDM interpretations of the CMS diphoton excess at 95 GeV*, *JHEP* **11** (2023) 017, [[2305.19716](#)].
- [42] T. Biekötter, S. Heinemeyer and G. Weiglein, *95.4 GeV diphoton excess at ATLAS and CMS*, *Phys. Rev. D* **109** (2024) 035005, [[2306.03889](#)].
- [43] A. Ahriche, M. L. Bellilet, M. O. Khojali, M. Kumar and A.-T. Mulaudzi, *Scale invariant scotogenic model: CDF-II W-boson mass and the 95 GeV excesses*, *Phys. Rev. D* **110** (2024) 015025, [[2311.08297](#)].
- [44] T.-K. Chen, C.-W. Chiang, S. Heinemeyer and G. Weiglein, *95 GeV Higgs boson in the Georgi-Machacek model*, *Phys. Rev. D* **109** (2024) 075043, [[2312.13239](#)].
- [45] J. Cao, X. Jia and J. Lian, *Unified Interpretation of Muon $g-2$ anomaly, 95 GeV Diphoton, and $b\bar{b}$ Excesses in the General Next-to-Minimal Supersymmetric Standard Model*, [2402.15847](#).
- [46] A. Arhrib, K. H. Phan, V. Q. Tran and T.-C. Yuan, *When Standard Model Higgs Meets Its Lighter 95 GeV Higgs*, [2405.03127](#).
- [47] K. Wang and J. Zhu, *95 GeV light Higgs in the top-pair-associated diphoton channel at the LHC in the minimal dilaton model*, *Chin. Phys. C* **48** (2024) 073105, [[2402.11232](#)].
- [48] W. Li, H. Qiao, K. Wang and J. Zhu, *Light dark matter confronted with the 95 GeV diphoton excess*, [2312.17599](#).
- [49] P. S. B. Dev, R. N. Mohapatra and Y. Zhang, *Explanation of the 95 GeV $\gamma\gamma$ and $b\bar{b}^-$ excesses in the minimal left-right symmetric model*, *Phys. Lett. B* **849** (2024) 138481, [[2312.17733](#)].
- [50] D. Borah, S. Mahapatra, P. K. Paul and N. Sahu, *Scotogenic $U(1)L\mu-L\tau$ origin of $(g-2)\mu$, W-mass anomaly and 95 GeV excess*, *Phys. Rev. D* **109** (2024) 055021, [[2310.11953](#)].
- [51] J. Cao, X. Jia, J. Lian and L. Meng, *95 GeV diphoton and $b\bar{b}^-$ excesses in the general next-to-minimal supersymmetric standard model*, *Phys. Rev. D* **109** (2024) 075001, [[2310.08436](#)].
- [52] U. Ellwanger and C. Hugonie, *Additional Higgs Bosons near 95 and 650 GeV in the NMSSM*, *Eur. Phys. J. C* **83** (2023) 1138, [[2309.07838](#)].
- [53] J. A. Aguilar-Saavedra, H. B. Câmara, F. R. Joaquim and J. F. Seabra, *Confronting the 95 GeV excesses within the $U(1)'$ -extended next-to-minimal 2HDM*, *Phys. Rev. D* **108** (2023) 075020, [[2307.03768](#)].
- [54] S. Ashanujjaman, S. Banik, G. Coloretti, A. Crivellin, B. Mellado and A.-T. Mulaudzi, *$SU(2)_L$ triplet scalar as the origin of the 95 GeV excess?*, *Phys. Rev. D* **108** (2023) L091704, [[2306.15722](#)].
- [55] J. Dutta, J. Lahiri, C. Li, G. Moortgat-Pick, S. F. Tabira and J. A. Ziegler, *Dark Matter Phenomenology in 2HDMS in light of the 95 GeV excess*, [2308.05653](#).
- [56] U. Ellwanger and C. Hugonie, *Nmssm with correct relic density and an additional 95 GeV Higgs boson*, *Eur. Phys. J. C* **84** (2024) 526, [[2403.16884](#)].
- [57] M. A. Diaz, G. Cerro, S. Dasmahapatra and S. Moretti, *Bayesian Active Search on Parameter Space: a 95 GeV Spin-0 Resonance in the $(B-L)$ SSM*, [2404.18653](#).

- [58] U. Ellwanger, C. Hugonie, S. F. King and S. Moretti, *NMSSM Explanation for Excesses in the Search for Neutralinos and Charginos and a 95 GeV Higgs Boson*, [2404.19338](#).
- [59] S. Y. Ayazi, M. Hosseini, S. Paktinat Mehdiabadi and R. Rouzbehi, *The Vector Dark Matter, LHC Constraints Including a 95 GeV Light Higgs Boson*, [2405.01132](#).
- [60] J. Lian, *The 95 GeV Excesses in the \mathbb{Z}_3 -symmetric Next-to Minimal Supersymmetric Standard Model*, [2406.10969](#).
- [61] J.-L. Yang, M.-H. Guo, W.-H. Zhang, H.-B. Zhang and T.-F. Feng, *Explaining the possible 95 GeV excesses in the $B - L$ symmetric SSM*, [2406.01926](#).
- [62] Z.-f. Ge, F.-Y. Niu and J.-L. Yang, *The origin of the 95 GeV excess in the flavor-dependent $U(1)_X$ model*, *Eur. Phys. J. C* **84** (2024) 548, [[2405.07243](#)].
- [63] S. Yaser Ayazi, M. Hosseini, S. Paktinat Mehdiabadi and R. Rouzbehi, *Vector dark matter and LHC constraints, including a 95 GeV light Higgs boson*, *Phys. Rev. D* **110** (2024) 055004, [[2405.01132](#)].
- [64] P. Janot, *The infamous 95 GeV $b\bar{b}$ excess at LEP: Two b or not two b ?*, [2407.10948](#).
- [65] K. Mosala, A.-T. Mulaudzi, T. Mathaha, P. Sharma, M. Kumar, B. Mellado et al., *The Observation of a 95 GeV Scalar at Future Electron-Positron Colliders*, [2407.16806](#).
- [66] J. Gao, J. Ma, L. Wang and H. Xu, *A 95 GeV Higgs boson and spontaneous CP-violation at the finite temperature*, [2408.03705](#).
- [67] J. Kalinowski and W. Kotlarski, *Interpreting 95 GeV di-photon/ $b\bar{b}$ excesses as a lightest Higgs boson of the MRSSM*, [2403.08720](#).
- [68] R. Benbrik, M. Boukidi and S. Moretti, *Superposition of CP-Even and CP-Odd Higgs Resonances: Explaining the 95 GeV Excesses within a Two-Higgs Doublet Model*, [2405.02899](#).
- [69] A. Khanna, S. Moretti and A. Sarkar, *Explaining 95 (or so) GeV Anomalies in the 2-Higgs Doublet Model Type-I*, [2409.02587](#).
- [70] P. Fileviez Perez, T. Han, G.-y. Huang, T. Li and K. Wang, *Neutrino Masses and the CERN LHC: Testing Type II Seesaw*, *Phys. Rev. D* **78** (2008) 015018, [[0805.3536](#)].
- [71] A. Arhrib, R. Benbrik, M. Chabab, G. Moultaka, M. C. Peyranere, L. Rahili et al., *The Higgs Potential in the Type II Seesaw Model*, *Phys. Rev. D* **84** (2011) 095005, [[1105.1925](#)].
- [72] S. F. King, *Models of Neutrino Mass, Mixing and CP Violation*, *J. Phys. G* **42** (2015) 123001, [[1510.02091](#)].
- [73] Y. Cai, T. Han, T. Li and R. Ruiz, *Lepton Number Violation: Seesaw Models and Their Collider Tests*, *Front. in Phys.* **6** (2018) 40, [[1711.02180](#)].
- [74] C.-H. Chen and T. Nomura, *Inert Dark Matter in Type-II Seesaw*, *JHEP* **09** (2014) 120, [[1404.2996](#)].
- [75] B. A. Ouazghour, A. Arhrib, R. Benbrik, M. Chabab and L. Rahili, *Theory and phenomenology of a two-Higgs-doublet type-II seesaw model at the LHC run 2*, *Phys. Rev. D* **100** (2019) 035031, [[1812.07719](#)].
- [76] M. J. Ramsey-Musolf, *The electroweak phase transition: a collider target*, *JHEP* **09** (2020) 179, [[1912.07189](#)].
- [77] B. A. Ouazghour, M. Chabab and K. Goure, *Higgs photon associated production in a two Higgs doublet type-II seesaw model at future electron-positron colliders*, *Eur. Phys. J. C* **84** (2024) 879, [[2403.07722](#)].
- [78] H. Bahl, T. Biekötter, S. Heinemeyer, C. Li, S. Paasch, G. Weiglein et al., *HiggsTools: BSM scalar phenomenology with new versions of HiggsBounds and HiggsSignals*, *Comput. Phys. Commun.* **291** (2023) 108803, [[2210.09332](#)].

- [79] P. Bechtle, S. Heinemeyer, O. Stål, T. Stefaniak and G. Weiglein, *HiggsSignals: Confronting arbitrary Higgs sectors with measurements at the Tevatron and the LHC*, *Eur. Phys. J. C* **74** (2014) 2711, [[1305.1933](#)].
- [80] P. Bechtle, S. Heinemeyer, O. Stål, T. Stefaniak and G. Weiglein, *Probing the Standard Model with Higgs signal rates from the Tevatron, the LHC and a future ILC*, *JHEP* **11** (2014) 039, [[1403.1582](#)].
- [81] P. Bechtle, S. Heinemeyer, T. Klingl, T. Stefaniak, G. Weiglein and J. Wittbrodt, *HiggsSignals-2: Probing new physics with precision Higgs measurements in the LHC 13 TeV era*, *Eur. Phys. J. C* **81** (2021) 145, [[2012.09197](#)].
- [82] P. Bechtle, O. Brein, S. Heinemeyer, G. Weiglein and K. E. Williams, *HiggsBounds: Confronting Arbitrary Higgs Sectors with Exclusion Bounds from LEP and the Tevatron*, *Comput. Phys. Commun.* **181** (2010) 138–167, [[0811.4169](#)].
- [83] P. Bechtle, O. Brein, S. Heinemeyer, G. Weiglein and K. E. Williams, *HiggsBounds 2.0.0: Confronting Neutral and Charged Higgs Sector Predictions with Exclusion Bounds from LEP and the Tevatron*, *Comput. Phys. Commun.* **182** (2011) 2605–2631, [[1102.1898](#)].
- [84] P. Bechtle, O. Brein, S. Heinemeyer, O. Stål, T. Stefaniak, G. Weiglein et al., *HiggsBounds – 4: Improved Tests of Extended Higgs Sectors against Exclusion Bounds from LEP, the Tevatron and the LHC*, *Eur. Phys. J. C* **74** (2014) 2693, [[1311.0055](#)].
- [85] P. Bechtle, D. Dercks, S. Heinemeyer, T. Klingl, T. Stefaniak, G. Weiglein et al., *HiggsBounds-5: Testing Higgs Sectors in the LHC 13 TeV Era*, *Eur. Phys. J. C* **80** (2020) 1211, [[2006.06007](#)].
- [86] C.-H. Chen and T. Nomura, *Two-Higgs-Doublet Type-II Seesaw Model*, *Phys. Rev. D* **90** (2014) 075008, [[1406.6814](#)].
- [87] B. A. Ouazghour and M. Chabab, *The two Higgs doublet type-II seesaw model: Naturalness and $B^- \rightarrow Xs\gamma$ versus heavy Higgs masses*, *Phys. Lett. B* **846** (2023) 138241, [[2305.08030](#)].
- [88] M. E. Peskin and T. Takeuchi, *Estimation of oblique electroweak corrections*, *Phys. Rev.* **D46** (1992) 381–409.
- [89] W. Grimus, L. Lavoura, O. M. Ogreid and P. Osland, *The Oblique parameters in multi-Higgs-doublet models*, *Nucl. Phys. B* **801** (2008) 81–96, [[0802.4353](#)].
- [90] **Particle Data Group** collaboration, R. L. Workman et al., *Review of Particle Physics*, *PTEP* **2022** (2022) 083C01.
- [91] **HFLAV** collaboration, Y. S. Amhis et al., *Averages of b -hadron, c -hadron, and τ -lepton properties as of 2021*, *Phys. Rev. D* **107** (2023) 052008, [[2206.07501](#)].
- [92] **LHC Higgs Cross Section Working Group** collaboration, D. de Florian et al., *Handbook of LHC Higgs Cross Sections: 4. Deciphering the Nature of the Higgs Sector*, **1610.07922**.
- [93] A. Djouadi, *The Anatomy of electro-weak symmetry breaking. II. The Higgs bosons in the minimal supersymmetric model*, *Phys. Rept.* **459** (2008) 1–241, [[hep-ph/0503173](#)].